Technical Report Documentation Page

1. Report No.	2. Government Accession No.	3. Recipient's Catalog No.
FHWA/TX-18/5-6921-01-R1		

4. Title and Subtitle	5. Report Date
APPLICATION OF A LASER SCANNING SYSTEM TO DYNAMIC FRICTION TEST SPECIMENS: CORRELATION BETWEEN TEXTURE AND FRICTION	Published: October 2018
	6. Performing Organization Code

7. Author(s)	8. Performing Organization Report No.
Edith Arámbula-Mercado, Emmanuel Fernando, Sheng Hu, and William Crockford	Report 5-6921-01-R1

9. Performing Organization Name and Address	10. Work Unit No. (TRAIS)
Texas A&M Transportation Institute The Texas A&M University System College Station, Texas 77843-3135	11. Contract or Grant No. Project 5-6921-01

12. Sponsoring Agency Name and Address	13. Type of Report and Period Covered
Texas Department of Transportation Research and Technology Implementation Office 125 E. 11th Street Austin, Texas 78701-2483	Technical Report: March 2018–August 2018
	14. Sponsoring Agency Code

15. Supplementary Notes

Project performed in cooperation with the Texas Department of Transportation and the Federal Highway Administration.
Project Title: Implementation of Laser Scanning System for Classification of Aggregate Texture
URL: http://tti.tamu.edu/documents/5-6921-01-R1.pdf

16. Abstract

In this implementation effort, a laser-based scanning system was adapted to test aggregates from five sources before and after Micro-Deval abrasion and embedded in a ring-shaped polyester material. Improvements to the ring-shaped specimen preparation procedure were identified. The Aggregate Ring Texturing System (ARTS) hardware and software were used on the aggregate ring-shaped specimens along with the dynamic friction tester (DFT) to obtain micro-texture and friction characteristics. The results allowed generating a model to predict friction at 60 km/h (DFT_{60}) from the micro mean profile depth results obtained with the ARTS. The aggregates from the various sources were ranked based on their texture and friction characteristics, and showed that igneous and gravel aggregates had superior micro-texture and friction performance as compared to dolomite and limestone. This type of analysis is geared toward improving the Texas Department of Transportation's existing surface aggregate classification system.

17. Key Words	18. Distribution Statement
Laser-Based Texture Measurements, Micro-Texture, Dynamic Friction Tester, Friction, Skid Resistance, Micro-Deval Abrasion	No restrictions. This document is available to the public through NTIS: National Technical Information Service Alexandria, Virginia http://www.ntis.gov

19. Security Classif. (of this report)	20. Security Classif. (of this page)	21. No. of Pages	22. Price
Unclassified	Unclassified	52	

Form DOT F 1700.7 (8-72) Reproduction of completed page authorized

APPLICATION OF A LASER SCANNING SYSTEM TO DYNAMIC FRICTION TEST SPECIMENS: CORRELATION BETWEEN TEXTURE AND FRICTION

by

Edith Arámbula-Mercado
Associate Research Engineer
Texas A&M Transportation Institute

Emmanuel Fernando
Senior Research Engineer
Texas A&M Transportation Institute

Sheng Hu
Associate Research Engineer
Texas A&M Transportation Institute

and

William Crockford
Research Engineer
Texas A&M Transportation Institute

Report 5-6921-01-R1
Project 5-6921-01
Project Title: Implementation of Laser Scanning System for Classification of Aggregate Texture

Performed in cooperation with the
Texas Department of Transportation
and the
Federal Highway Administration

Published: October 2018

TEXAS A&M TRANSPORTATION INSTITUTE
College Station, Texas 77843-3135

DISCLAIMER

This research was performed in cooperation with the Texas Department of Transportation (TxDOT) and the Federal Highway Administration (FHWA). The contents of this report reflect the views of the authors, who are responsible for the facts and the accuracy of the data presented herein. The contents do not necessarily reflect the official view or policies of the FHWA or TxDOT. This report does not constitute a standard, specification, or regulation.

The United States Government and the State of Texas do not endorse products or manufacturers. Trade or manufacturers' names appear herein solely because they are considered essential to the object of this report.

ACKNOWLEDGMENTS

This project was conducted in cooperation with TxDOT and FHWA. The authors thank Richard Izzo, Project Director, and other members of the Project Monitoring Committee, in particular, Edward Morgan and Jeffrey Perabo for their support and guidance. The authors also acknowledge Joe Adams, Darrin Jensen, and Joanne Steele for their service as project managers.

TABLE OF CONTENTS

Page

List of Figures ..... **viii**
List of Tables ..... **ix**
Chapter 1. Introduction **1**
Chapter 2. Laboratory Experiment **3**
2.1. Micro-Deval Abrasion 3
2.2. Ring-Shaped Specimen Preparation 4
2.3. Dynamic Friction Tester 5
Chapter 3. Aggregate Ring Texturing System **7**
3.1. Overview 7
3.2. Hardware 9
3.3. Software 9
3.4. Recommendations to the User 11
Chapter 4. Data Analysis **15**
4.1. Data Processing 15
4.2. Comparison between Forward and Backward Scans 18
4.3. Comparison between BMD and AMD Texture Measurements 22
4.3. Relationship between Friction And Aggregate Micro-texture 22
4.4. Relative Ranking of Aggregate Types 29
Chapter 5. Conclusions and Recommendations **33**
5.1. Ring-Shaped Specimen Preparation 33
5.2. Aggregate Ranking 34
References **35**
Appendix: DFT and Micro-Texture Data on TxDOT Aggregate Ring Specimens **37**

LIST OF FIGURES

Page

Figure 1. Micro-Deval Test; (a) Test Specimen and Steel Balls before Saturation, (b) Setup during Testing. 4
Figure 2. Ring-Shaped Specimen; (a) HDPE Template and (b) Cured Specimen. 5
Figure 3. DFT Test; (a) Apparatus Side View (*2*), (b) Apparatus bottom View (*2*), and (c) TxDOT Setup. 6
Figure 4. DFT Output for Run 1, 2, and 3. 6
Figure 5. Power Inlet Components. 8
Figure 6. Power Inlet Module Packaging (Power Switch Is Intended to Be on Left Side When Looking at It from the Front). 8
Figure 7. Laser Arm Enclosure. 9
Figure 8. Operator Control Panel. 11
Figure 9. Keyence Navigator Software. 12
Figure 10. Advanced Setting Option. 13
Figure 11. Settings Available for Modification (see *Sure*Step for Additional Information). 13
Figure 12. ARTS Data Processor User Interface. 15
Figure 13. Example of a 3D Graph as Generated by the ARTS Data Processor. 18
Figure 14. Comparison between Forward and Backward ARTS Laser Scans; (a) Aggregates after Micro-Deval Abrasion and (b) Aggregates before Micro-Deval Abrasion. 20
Figure 15. Comparison of 3D Graph from ARTS Laser Scans; (a) Forward Scan and (b) Backward Scan. 21
Figure 16. Comparison of the ARTS μMPD Values for Aggregates before Micro-Deval Abrasion and after Micro-Deval Abrasion. 22
Figure 17. Comparison of Predicted vs. Measured DFT_{60} 25
Figure 18. Plot of Residuals vs. Predicted DFT_{60}. 27
Figure 19. Plot of Residuals vs. μMPD. 28
Figure 20. Plot of Cook's D Statistic for Each Observation in DFT-μMPD Data Set. 28
Figure 21. Comparison of Averages of Measured and Predicted Values of DFT_{60}. 31

LIST OF TABLES

Page

Table 1. Central Tendency and Dispersion Statistics on DFT_{60} 23
Table 2. Central Tendency and Dispersion Statistics on Aggregate Micro-Texture (μMPD) 23
Table 3. Results from Statistical Tests of Significance between BMD and AMD Aggregate Properties. 24
Table 4. Model Parameter Estimates Determined from Regression Analysis. 26
Table 5. VIFs Determined from Regression Analysis. 29
Table 6. Results from Testing Significance of Differences between Means of Measured DFT_{60} Values. 30
Table 7. Central Tendency and Dispersion Statistics on Predicted Values of DFT_{60} 31
Table 8. Results from Testing Significance of Differences between Means of Predicted DFT_{60} Values. 32

CHAPTER 1. INTRODUCTION

The lack of pavement friction causes vehicles to skid and run off the road. In 2016, single vehicle run-off-the-road crashes resulted in 1,293 deaths on Texas highways. The Texas Department of Transportation (TxDOT) highway safety improvement program evaluated the cost of one roadway fatality or one incapacitating injury at approximately $3.3 million (*1*). If building better skid-resistant pavement surfaces could reduce fatalities by 1 percent, the potential annual reduction in societal cost, given the number of run-off-the-road fatalities in 2016, would be significant.

With the goal of improving the measurement of aggregate characteristics and classification, a laser-based system to measure aggregate properties that was developed under TxDOT project 0-6921: *Use of Lasers for Laboratory Measurements of Aggregate Shape, Angularity, and Texture* was initially implemented as part of this study. The laser-based system was adapted to scan ring-shaped specimens specifically prepared to evaluate friction characteristics via the dynamic friction tester (DFT) as part of the Aggregate Quality Monitoring Program. Individual aggregate particles in original state and after Micro-Deval abrasion were used to prepare the ring-shaped specimens.

The objectives of this study included: 1) compiling a database of friction and texture properties of aggregates commonly used on Texas roadways, 2) processing the data to determine a possible relationship between texture and friction, 3) ranking the scanned aggregates based on observed texture and friction values, and 4) identifying improvements to TxDOT's existing surface aggregate classification (SAC) system.

Because of the nature of the test specimens, modifications to the laser system originally developed under TxDOT project 0-6921 had to be considered. For the hardware, the laser-based system had to rotate to scan the surface of the ring-shaped specimen. In addition, the software was modified to accommodate the scan of a surface with various aggregate particles embedded in it instead of analyzing discrete aggregate particles as done in TxDOT project 0-6921.

TxDOT's Geotechnical, Soils and Aggregates Branch prepared the ring-shaped specimens using various aggregate sources and performed the scans with the DFT and laser-based system. The data were sent to the research team for processing. A comparison between DFT and laser-based texture measurements was performed with the goal of developing a relationship between the two variables.

The modifications to the laser-based system are discussed in Chapter 2. The experimental plan is described in Chapter 3, and Chapter 4 presents the comparison between the laser-based texture and the friction measurements. Chapter 5 offers conclusions and recommendations.

CHAPTER 2. LABORATORY EXPERIMENT

For the evaluation of texture with the laser-based system and friction with the DFT, TxDOT prepared ring-shaped specimens. Several aggregate sources were tested for this study including:

- Dolomite.
- Gravel.
- Igneous.
- Limestone.
- Sandstone.

As part of the Aggregate Quality Monitoring Program, a sample of aggregates from each source was subjected to Micro-Deval abrasion. Further, the original and abraded aggregates were used to prepare the ring-shaped specimens and subjected to testing with the laser-based system first, followed by the DFT. The test procedures are described next.

2.1. MICRO-DEVAL ABRASION

TxDOT's aggregate laboratory subjected aggregate samples from each source to Micro-Deval abrasion following standard test method TEX-461-A: *Degradation of Coarse Aggregate by Micro-Deval Abrasion*. The procedure requires a 1,500 ± 5 gram sample of aggregates that have been sieved, washed, and oven dried to constant weight at a temperature of 230°F (110°C). The container used for testing is prepared by adding 5,000 ± 5 grams of stainless steel balls. These are placed prior to putting the aggregate test sample in the container to minimize abrasion (see Figure 1a). After introducing the aggregate sample, 2,000 ± 500 ml of water is poured in the container to saturate the sample for a minimum of 1 hour. After saturation, the container is placed on its side in the Micro-Deval apparatus and tested at 100 ± 5 rpm for 105 ± 1 minute in the case of bituminous aggregates (see Figure 1b).

After the established test time, sieve No. 4 (4.75 mm) and sieve No. 16 (1.18 mm) are stacked and used to decant the aggregate sample. The sample is then washed until the water running from the stack of sieves is clear and all material passing sieve No. 16 has been removed. A magnet is then used to remove the stainless steel balls from the aggregate test sample. Subsequently, the remaining aggregate is oven dried overnight at 230°F (110°C), and constant weight after drying verified. The initial aggregate sample weight and oven dry weight after the Micro-Deval test procedure are used to calculate the percent loss due to abrasion.

(a) **(b)**

Figure 1. Micro-Deval Test; (a) Test Specimen and Steel Balls before Saturation, (b) Setup during Testing.

2.2. RING-SHAPED SPECIMEN PREPARATION

The procedure TxDOT's Geotechnical, Soils and Aggregates Branch used to prepare the ring-shaped specimens consisted of several steps. First, the before Micro-Deval (BMD) and after Micro-Deval (AMD) ¼ inch (6.35 mm) aggregates samples were received from the aggregate laboratory. Then, the ring was built on a high-density polyethylene (HDPE) template (see Figure 2a) by filling ½ inch (12.7 mm) deep circular channel with polyester and using a 1/8 inch (3.18 mm) notched out plastic spatula to remove the polyester to a level approximately 1/8 inch (3.18 mm) below the surface of the HDPE template. Prior to filling the channel with polyester, a debonding grease was applied to the surface of the channel so the ring could be easily removed from the HDPE template after testing. A ratio of 0.8 lb (351 gram) of polyester to 0.06 ounce (1.7 gram) methyl ethyl ketone peroxide was required to allow enough time to place and roll the aggregates before the polyester set. Next, the HDPE template was placed on a turn table and slowly rotated while the aggregates were deposited with a scoop of the same width as the channel. Aggregate particles were then manually placed in areas of the ring that did not receive a tight arrangement of aggregates. Further, a hard rubber roller, wider than the annular ring, was rolled over the full circumference of the ring until the aggregate was flush with the surface of the HDPE template. Finally, the ring-shaped specimen is left to cure for about 1 hour before testing. Figure 2b shows a finished specimen.

(a) **(b)**

Figure 2. Ring-Shaped Specimen; (a) HDPE Template and (b) Cured Specimen.

2.3. DYNAMIC FRICTION TESTER

After the ring-shaped specimen was cured, it was subjected to a series of tests. First, the laser-based system was employed to obtain the micro mean profile depth (μMPD). The characteristics of the laser-based system, henceforth called the aggregate ring texturing system (ARTS), are described in Chapter 3. After obtaining texture, the DFT equipment is setup on top of the HDPE template with the cured ring-shaped specimen and tested in triplicate (i.e., three consecutive runs).

The DFT is a portable tool for measuring the dynamic friction coefficient. In addition to the apparatus shown in Figure 3a, a steel water bucket connects to a nozzle on the DFT through a plastic hose as shown in Figure 3c. The bucket provides gravity-fed water to the DFT, which is then discharged through the bottom of the unit during testing to wet the pavement. A portable processing unit and laptop computer connects to the DFT to control and monitor the apparatus and collect the test results. The bottom of the DFT apparatus has three rubber sliders that are spring-mounted to the bottom of a disk with a diameter of 13.2 inch (335 mm) (see Figure 3b). During testing, the disk is held above the pavement as the electric motor in the DFT spins the disk so that the tangential velocity of the sliders reaches 56 mph (90 km/h). The DFT sprays water onto the pavement. Upon reaching the target testing velocity, the motor disengages and the rubber sliders are lowered onto the pavement surface. After contact with the pavement surface, the disk maintains a constant load and begins to decelerate. A transducer on the disk measures the friction force and accompanying speed of the disk. From these data, a continuous spectrum of the resulting friction coefficient is generated from 56 to 0 mph (90 to 0 km/h). Of this spectrum, the friction coefficients at 12, 24, 36, and 48 mph (20, 40, 60, and 80 km/h) are reported, and the value at 60 km/h (36 mph) or DFT_{60} used for further analysis.

Figure 3. DFT Test; (a) Apparatus Side View (*2*), (b) Apparatus bottom View (*2*), and (c) TxDOT Setup.

An analysis of the DFT data revealed a consistent decreasing trend in the DFT_{60} values with each consecutive run as shown in Figure 4. This is possibly due to the ring-shaped specimen being dry when the first DFT scan is performed, but wet during the 2nd and 3rd runs after water had been applied to the surface of the specimen as part of the test procedure. For data analysis, the averages of the three runs were considered, according to TxDOT's current practice.

Figure 4. DFT Output for Run 1, 2, and 3.

CHAPTER 3. AGGREGATE RING TEXTURING SYSTEM

The laser-based system developed under TxDOT project 0-6921 was modified to accommodate scanning of the ring-shaped specimens. The ARTS hardware and software components are described in this chapter.

3.1. OVERVIEW

The ARTS is designed to work on ring-shaped specimens prepared for DFT evaluation, collecting micro-texture mean profile depth (μMPD) measurements on the same aggregate samples. There are four main components of the system:

1) Panasonic Toughbook CF-VEK331LM (7KTSA09354).
2) Operation and setup software comprising:
   a) Keyence laser operation/monitoring software (LJ-Navigator).
   b) Laser/Stepper motor synchronization software (ARTS).
   c) *Sure*Step Pro software used to set up the micro-stepping drive and the stepper motor (this software is not normally used by the operator).
3) A power inlet and signal conditioning module (Figure 5 and Figure 6) comprising:
   a) A duplex 110V main power switch and unswitched outlet (e.g., for a computer power supply).
   b) An AC-DC converter to convert to 24VDC to drive the electronics.
   c) A DC-DC converter to convert 24VDC to 5VDC to provide signal power to the stepper drive.
   d) A fuse holder (recommended fuse 4A 3AG delay).
   e) An advanced micro-stepping drive.
   f) The Keyence laser power/signal processing module.
4) Keyence laser system with the LJ-V7080 laser head (68610206) mounted inside a partially transparent enclosure (Figure 7) on an arm that is rotated by a stepper motor.

   The laser and motor cables are intended to come out the back of the enclosure. The laser should be on the right and the bar approximately parallel to the front bar with slack cable prior to starting testing.

   The height of the laser above the surface of the aggregate can be adjusted a slight amount with the feet or the mounting blocks at each end of the brass motor support bar. However, no adjustment should be needed after initial setup. There is also a circular level mounted in the brass bar for reference.

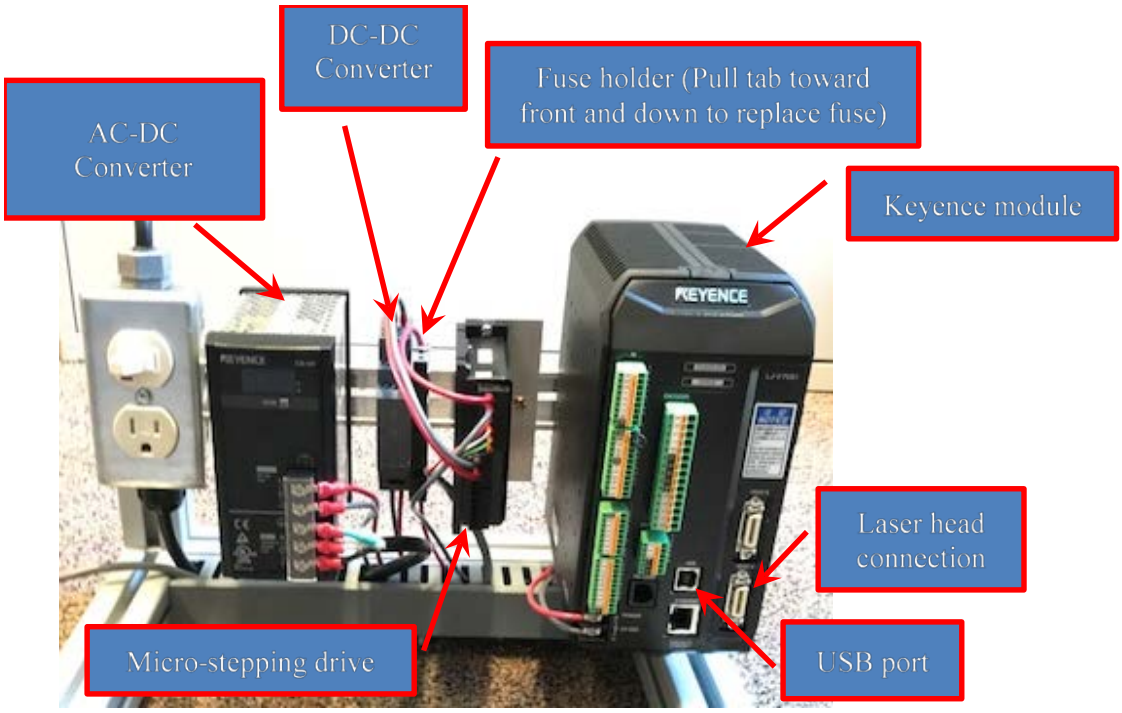

Figure 5. Power Inlet Components.

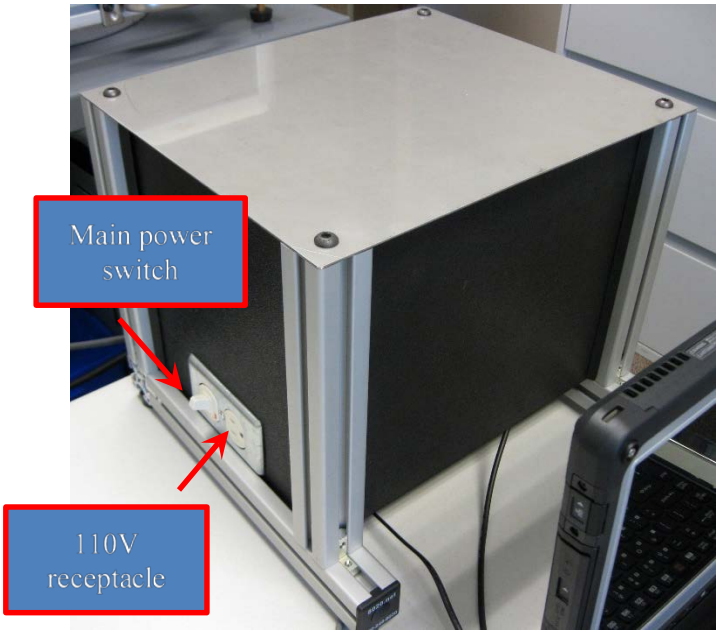

Figure 6. Power Inlet Module Packaging (Power Switch Is Intended to Be on Left Side When Looking at It from the Front).

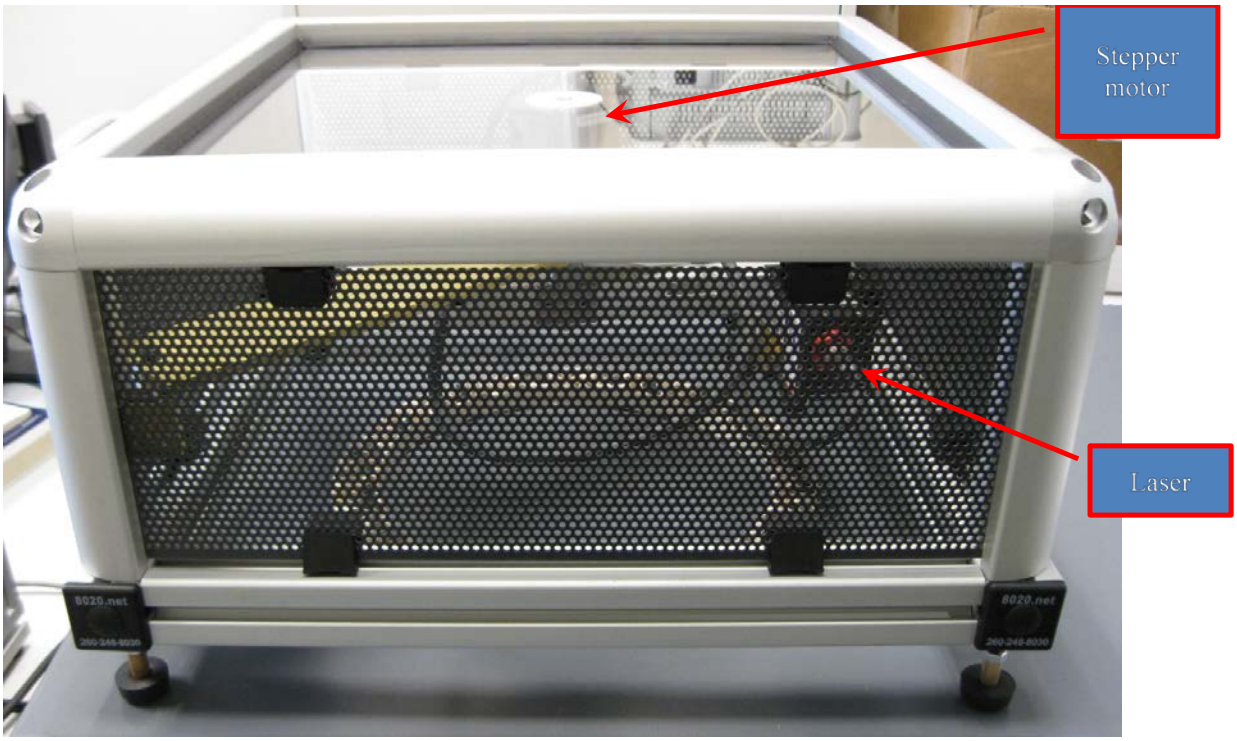

Figure 7. Laser Arm Enclosure.

3.2. HARDWARE

Plug the power inlet/signal conditioning module into a standard 110VAC wall outlet. There are four additional cables that must be connected for the system to work:

1. Connect the RS232 (D Sub connector) cable into the computer. The other end of this connector is an RJ11 (6P4C) connector (similar to a phone connector) that is plugged into the bottom of the micro-stepping drive.
2. Connect the USB cable into the computer. The other end is connected to the Keyence signal processing module.
3. Connect the stepper motor cable with the small black in-line connector (release by pressing the small tab and pulling apart) near the back of the laser arm enclosure.
4. Connect the laser cable to the bottom (Laser A) high density D connector.

3.3. SOFTWARE

The Keyence LJ- V7080 line laser and the *Sure*Step motor (STPMTRH23079) are synchronized to rotate the laser while collecting the DFT aggregate profile information. The LJ-Navigator 2 application (Keyence Navigator) that comes with the LJ-V7080 line laser is automated to perform the data collection.

The micro-texture measurement process includes the following steps:

1. Connect the USB cable (laser control cable) and RS-232 cable (motor control cable) to Panasonic Toughbook laptop computer.
2. Turn on the power of ARTS system (Figure 6).
3. Double click the ARTS icon on the desktop to start the data collection program.
4. The program will automatically prepare the communication with *Sure*Step motor and the Keyence Navigator software. Once done, the initiation status on the screen will show "Initiation Complete" (Figure 8).
5. Input the data folder and file name (system asks whether to overwrite if the file already exists).
6. Check if the laser is in a good start position. A good start position means the laser can be rotated 360° clockwise without winding too much cable around the shaft. If the laser position is not good, click the rotate buttons on the screen to do a manual adjustment.
7. Click the Scan button to start the data collection. The laser will rotate first 360° one direction (forward) and then 360° the reverse direction (backward).
8. Two separate profile data files will be collected. During the process, the Keyence Navigator software will be automated by the ARTS control program. Interruptions during this process will cause loss of data and the test will need to be run again.
9. In the case of some unpredicted situation, the user can click the red button Emergency Stop to stop both the motor rotating and the laser data collection.
10. When the test is finished, click the Quit button on the ARTS user screen. Both the Keyence Navigator program and the ARTS program will be closed.
11. Turn off the power of ARTS system.

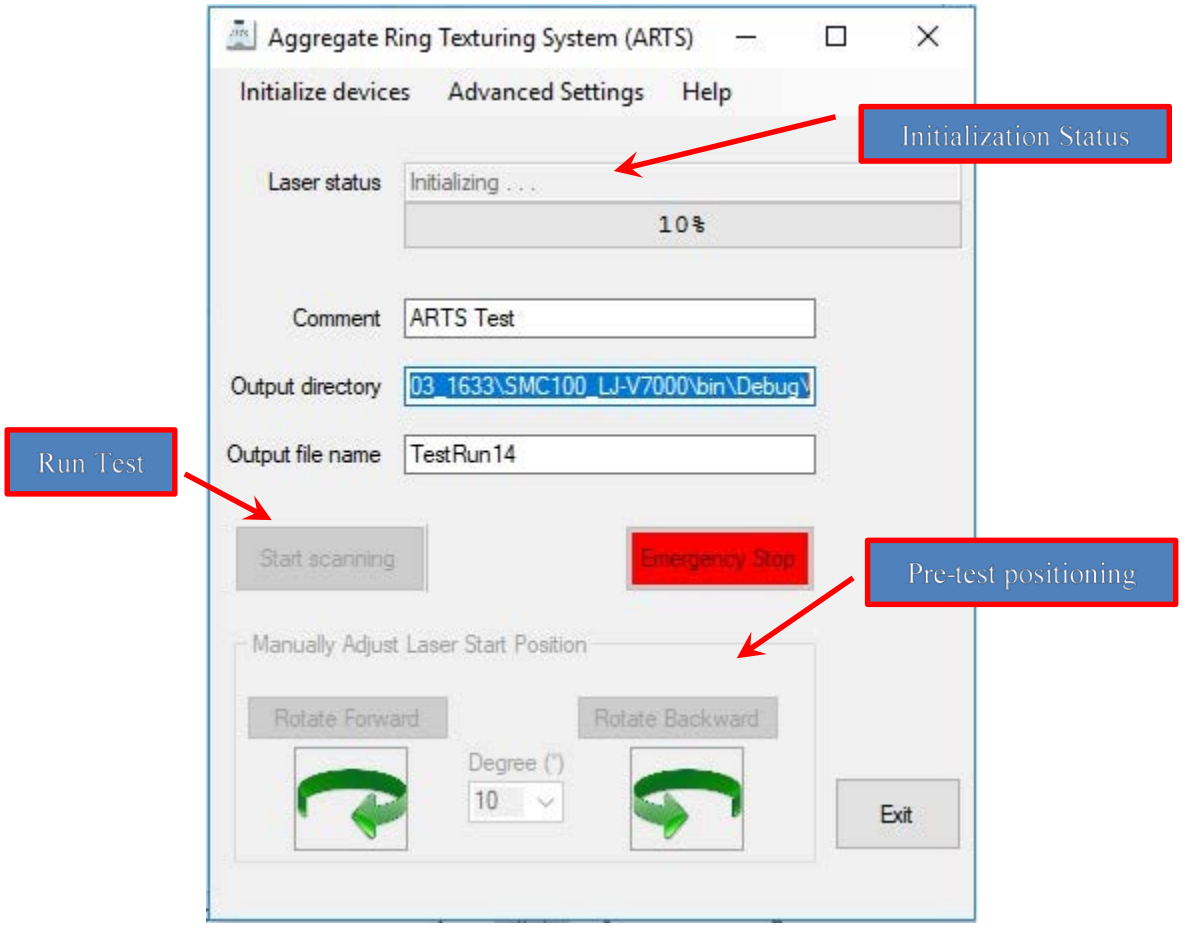

Figure 8. Operator Control Panel.

3.4. RECOMMENDATIONS TO THE USER

It is not recommended that the user reorganize the Keyence Navigator software screens including screen size or locations since these operations may affect the automation process. The screens should be displayed as shown in Figure 9.

The Keyence laser has a measuring height range, which is between approximately 2.5 and 3.5 inches (63.5–88.9 mm) and an actual full range of 3.15 ± 0.91 inch (80 ± 23.1 mm). The user is advised to not adjust the height of the bar or the support feet since it will affect the laser measuring height except when setting up the first time or to handle larger aggregate particles that may exceed the measuring height range.

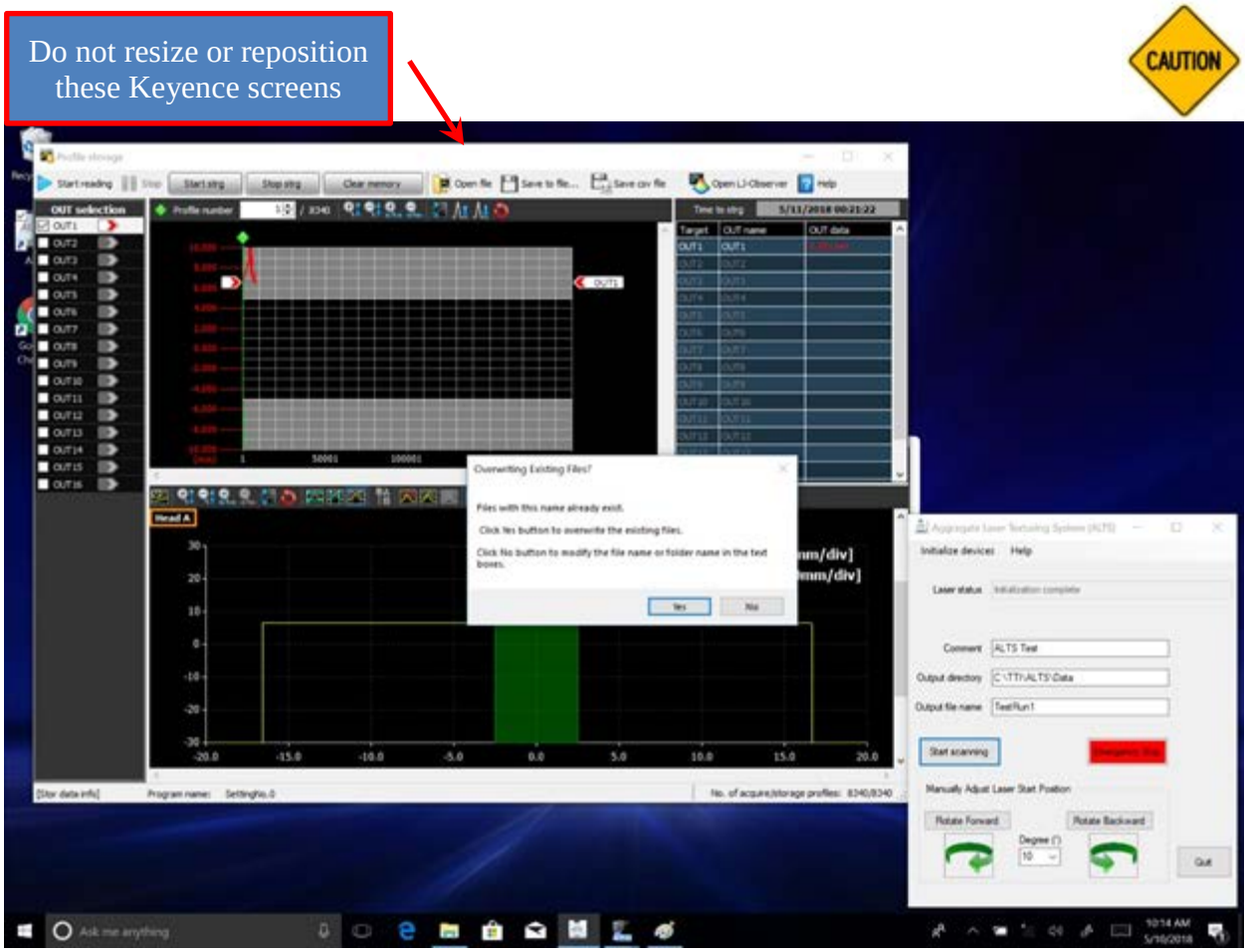

Figure 9. Keyence Navigator Software.

The software has the capability to customize the operation of the system (see Figure 10). This should only be done by qualified personnel because it can significantly alter the quality of the resulting data. The most commonly customized features of the system are the Keyence data acquisition rate available in the Keyence software (see Keyence software documentation) and the motor operation parameters available in the ARTS software (see Figure 11). The Advanced Settings screen in the ARTS software is password protected with a default of 123.

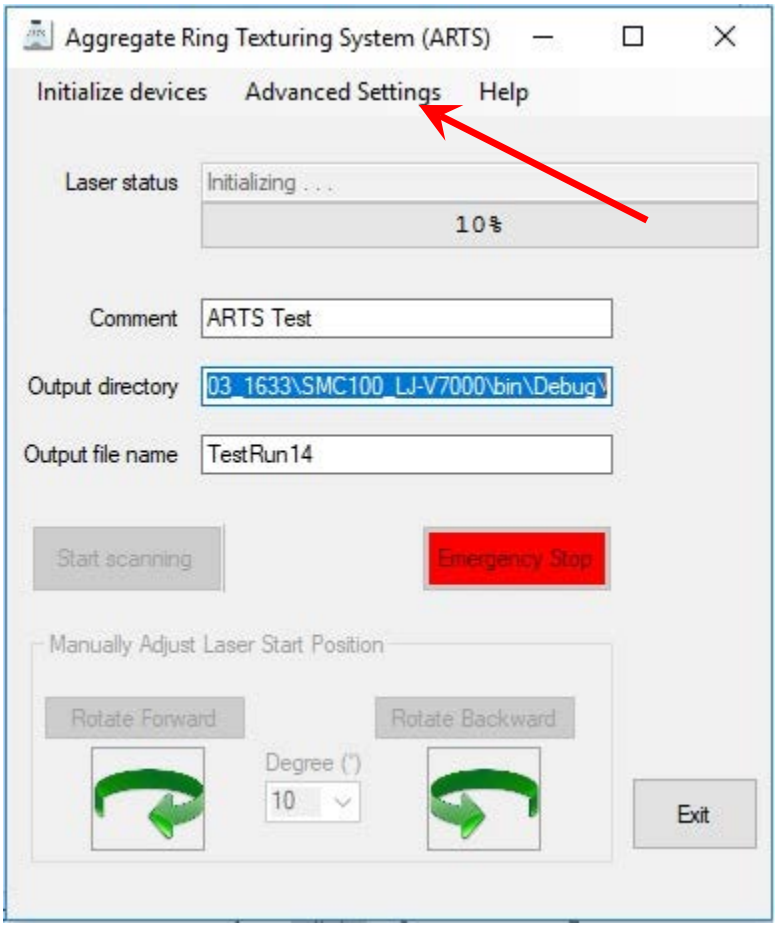

Figure 10. Advanced Setting Option.

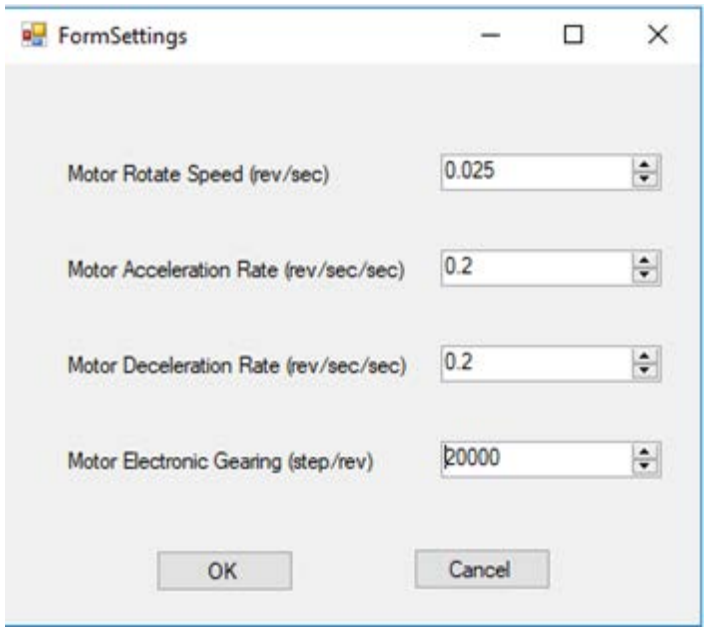

Figure 11. Settings Available for Modification (see *Sure*Step for Additional Information).

CHAPTER 4. DATA ANALYSIS

In this chapter, a description of the software developed to process the data acquired with the laser-based system ARTS is described, as well as the comparison between μMPD and DFT results.

4.1. DATA PROCESSING

A data processing software was developed for the purpose of analyzing the laser data acquired with the ARTS. Figure 12 shows the main screen of the software.

Figure 12. ARTS Data Processor User Interface.

Pushing the *F1* button opens the software User Guide; when the mouse moves across the screen, a note will show near the cursor reading: “Please push *F1* for help.”

To process the laser data and calculate the μMPD, the user action needed is double-clicking a selected raw laser data file. The program will automatically calculate the ring μMPD, and document details such as μMPD of each scan line in the intermediate file. The user can also view these details on the screen by changing the values in the corresponding drop-down boxes.

The following provides notes of the user interface and definitions of parameters. The item numbers listed below relate to the numbers highlighted in Figure 12.

1. Choose Laser Data Folder Button:

    - Click this button.
    - Choose a folder that has raw laser data files from the Browse for Folder Dialogue.
    - Click OK button.
    - All the raw laser data files names will be listed in the list box under the Choose Laser Data Folder Button.

2. Raw Laser Data File List Box:

    - Double click the file name to be analyzed.
    - A progress bar will show to indicate the analysis process.
    - After the analysis is completed, the File text box will show the full file name of the analyzed raw data file.
    - A folder with the raw data file name will be created. Two files will be in this folder: one file name ends with "_processed" and the other ends with "_MPD." The analysis is based on the "processed" file generated after removing invalid laser readings from the raw laser data file. The "_MPD" file documents all line MPD values.

3. Settings:

    - Left Margin of Line Scan, the distance between the leftmost point of the scan line and the left side of the test ring, in mm. The preset value is 4 mm.
    - Right Margin of Line Scan, the distance between the right side of the test ring and the rightmost point of the san line. The preset value is 8 mm.
    - Laser Scan Time Before Rotating, the time between start of laser emission and laser arm rotation (controlled by the stop motor). The preset value is 2 seconds.
    - Laser Scan Time After Rotating, the time between stoppage of laser arm rotation (controlled by the step motor) and end of laser mission. The preset value is 1 second.
    - Smoothing Based on Moving Average Points, the points used to calculate the moving average for the laser readings and to remove some potential spikes (unreasonable laser readings). The preset value is 10.
    - Base Line Offset, the depth from the ring ceiling height, used to determine the base line with which to identify the aggregates in the ring. The preset value is 1.2 mm.
    - Usually these settings do not need to be changed unless the test ring or test conditions have significantly changed.

4. Analysis Results:

    - Total Lines, the total analyzed laser scan lines.
    - Ring Micro MPD, the final average micro MPD value of all the scan lines, in mm.

- Standard Deviation, the standard deviation of MPD values of all the scan lines, in mm.
- Line No., the number of scan line. Users can select a line to view the corresponding line MPD value, the line measurement plot, and other detailed information. The range of the Line No is from 1 to the Total Lines.
- Line Laser Rotating Degree, the laser equipment rotating (controlled by the step motor) degree, from 0 to 360°. The Line No 1 corresponds to 0°, and the Total Lines corresponds to 360°.
- Line MPD, the micro MPD value of the specified laser scan line. It is an average value among the MPD values of the identified stones.

5. Line Laser Measurement Plot:

    - Line Laser Measurements, shows each measured laser point location in the scan line and the corresponding elevation reading.
    - Base Line, shows the line which is used to identify stones.
    - Smoothed Measurements, shows the line determined by the moving average method.
    - Segment, the red triangle marker shows the current segment for the computation of segment MPD.

6. Stone and Segment MPD Results:

    - Stone No. on the Line, the number of the stone identified by the base line. If the user chooses a different Stone No., the red triangle maker location in the "Line Laser Measurement Plot" will change accordingly.
    - Stone MPD on the Line, the MPD value of the stone identified, mm. The stone MPD value is the average of the stone segment MPD values. If the user chooses a different Stone No., this value will change accordingly.
    - Segment No. on the Stone, the number of the segment on the stone. If the user chooses a different Segment No., the red triangle maker location in the "Line Laser Measurement Plot" will change accordingly. If the user chooses a different Segment No., this value will change accordingly.
    - Left Half Segment MPD, the difference between the peak value of the left half segment and the average level, mm. If the user chooses a different Segment No., this value will change accordingly.
    - Right Half Segment MPD, the difference between the peak value of the right half segment and the average level, mm. If the user chooses a different Segment No., this value will change accordingly.
    - Segment MPD on the Stone, the segment MPD values, which is the average of Left and Right Half Segment MPD values. If the user chooses a different Segment No., this value will change accordingly.

7. Segment Plot:
    - Segment Points After Detrending, shows the detrended measured laser point locations of the selected segment and the corresponding elevation readings. Detrending removes the influence of the slope.
    - Average Line, shows the average level of the detrended segment profile.
8. Show 3D Graph Button:
    - Click this button.
    - This button will turn gray (disabled) while the graph is being generated.
    - The 3D graph of the stone surface plot starting from the user-selected scan line will pop up, as seen in the following figure.
    - Once the graph is generated, the button is enabled again. Figure 13 shows an example of a 3D graph.

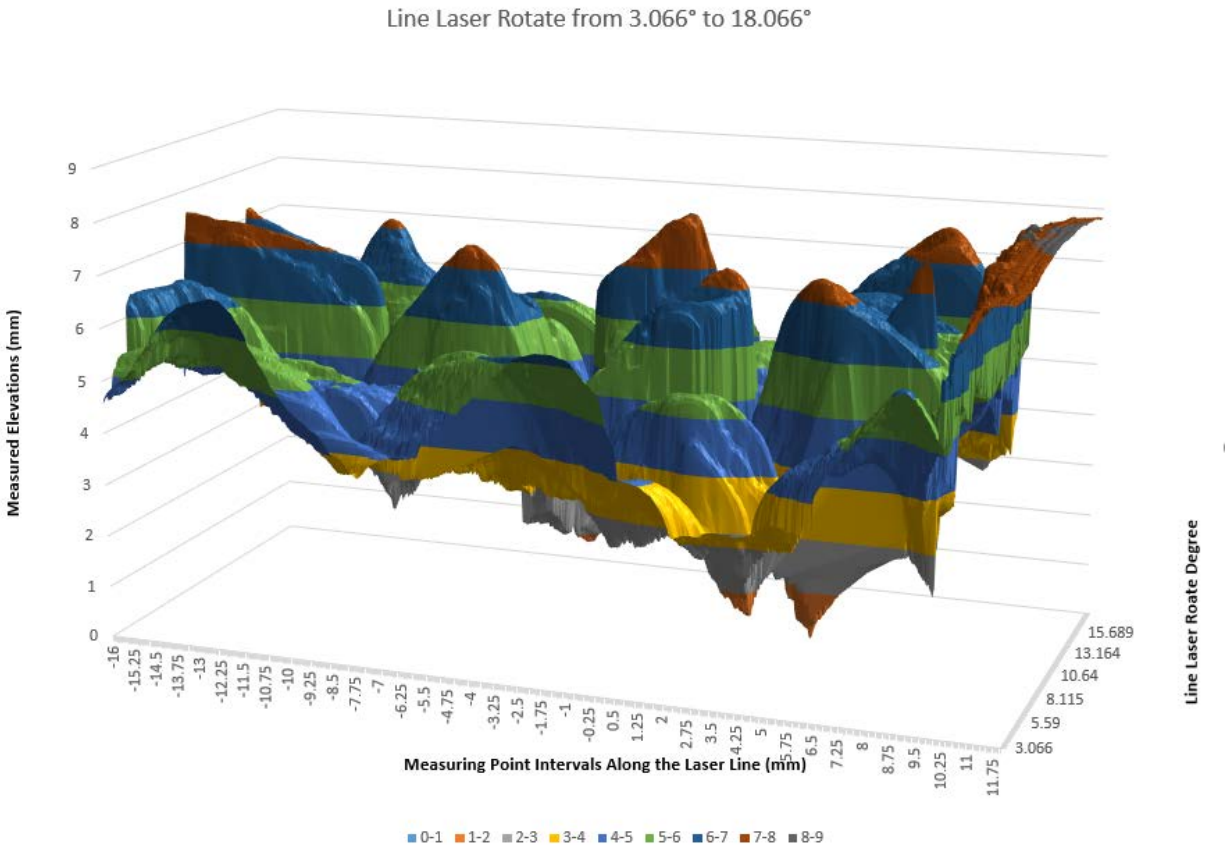

Figure 13. Example of a 3D Graph as Generated by the ARTS Data Processor.

4.2. COMPARISON BETWEEN FORWARD AND BACKWARD SCANS

During the operation of the ARTS, two scans are acquired when the ring-shaped specimen is scanned: one as the laser bar moves in one direction (labeled forward) and another as the laser

returns to its original position (labeled backward). It was relevant to compare these two results to assess the repeatability of the two results.

As shown in Figure 14, the computed μMPD from corresponding forward and backward scans show excellent agreement, aligning right on top of the 45° equality line. There is no indication of a systematic bias between the data from corresponding forward and backward laser scans. In addition, a side-by-side comparison using the 3D graph of the ARTS Data Processor also illustrates the equivalency between the forward and backward scans as shown in Figure 15. Therefore, the average from the two results was reported as the ring-shaped specimen μMPD and used in the comparison between texture and friction described next.

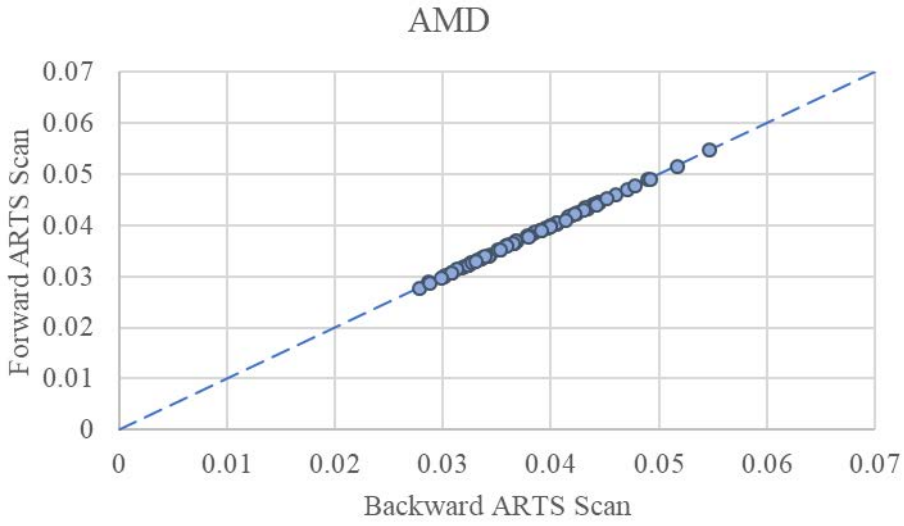

(a)

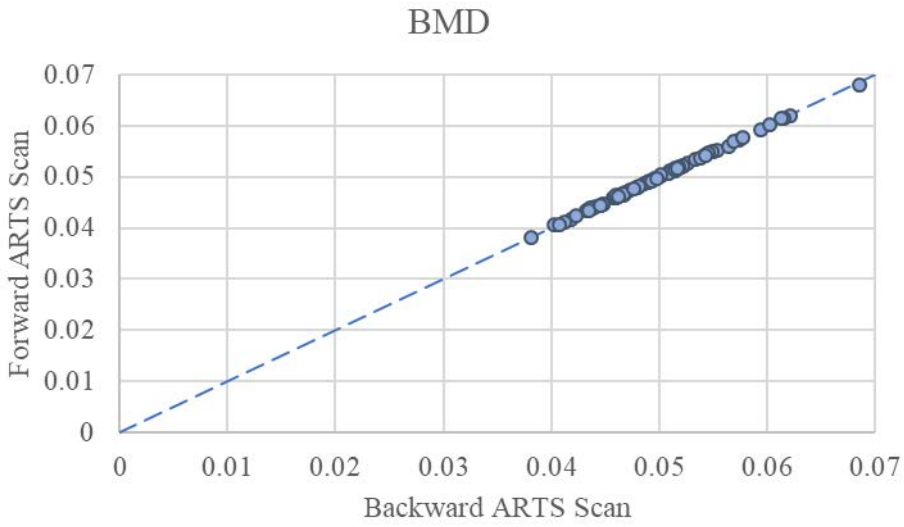

(b)

Figure 14. Comparison between Forward and Backward ARTS Laser Scans; (a) Aggregates after Micro-Deval Abrasion and (b) Aggregates before Micro-Deval Abrasion.

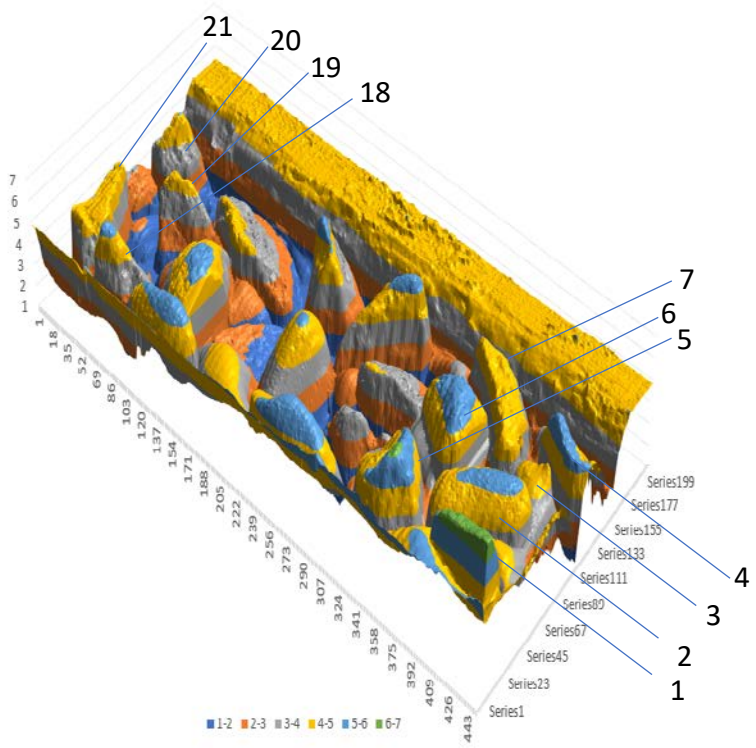

(a)

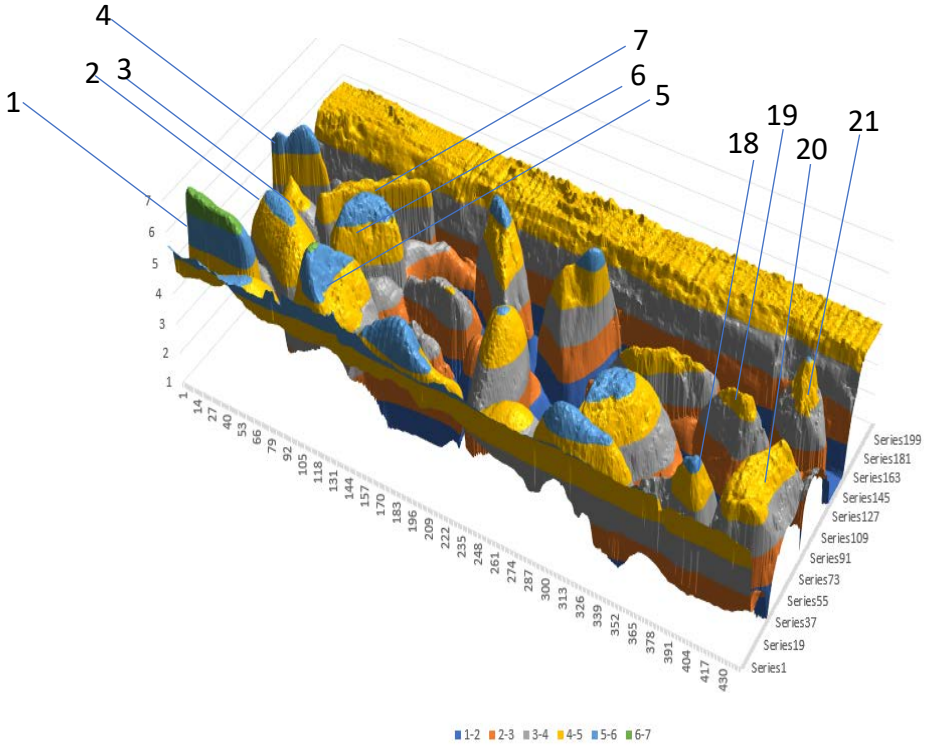

(b)

Figure 15. Comparison of 3D Graph from ARTS Laser Scans; (a) Forward Scan and (b) Backward Scan.

4.3. COMPARISON BETWEEN BMD AND AMD TEXTURE MEASUREMENTS

It was considered relevant to also assess the difference between micro-texture for the aggregates in original condition (i.e., BMD) and those subjected to the standard abrasion test procedure (i.e., AMD). When comparing these two results for all aggregate sources as shown in Figure 16, most of the BMD μMPD results were larger than the AMD μMPD results, as expected. Figure 16 shows that most of the AMD μMPD results align below the 45° equality line (i.e., dashed line), implying lower micro-texture after abrasion.

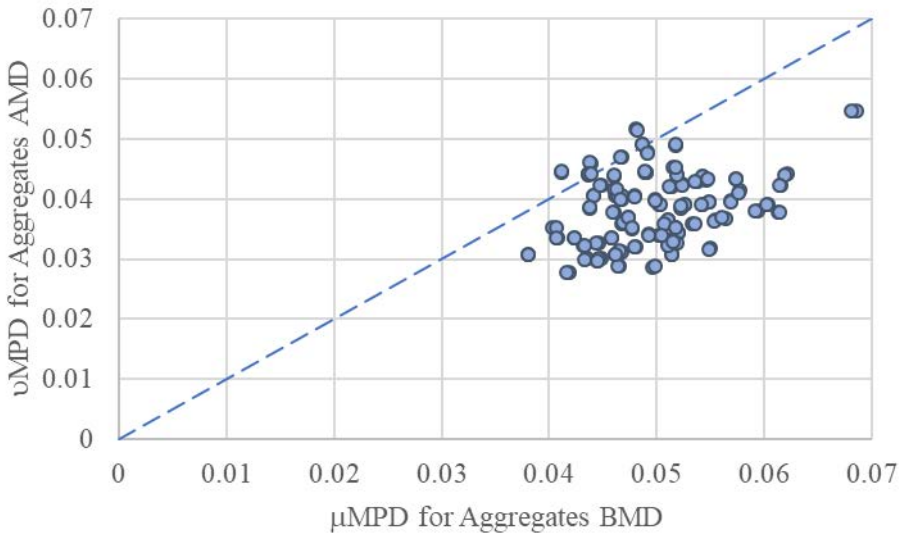

Figure 16. Comparison of the ARTS μMPD Values for Aggregates before Micro-Deval Abrasion and after Micro-Deval Abrasion.

4.3. RELATIONSHIP BETWEEN FRICTION AND AGGREGATE MICRO-TEXTURE

The data from the DFT and ARTS system collected by TxDOT on the ring-shaped specimens were provided to the research team along with information identifying the different aggregates sources. TTI processed the ARTS test data to determine the aggregate micro-texture for the given ring-shaped specimen. This analysis, the steps of which are detailed in Section 4.1, detects the aggregates in each laser scan and computes the μMPD only for the aggregates detected in the scan (i.e., the polyester material within which the aggregates are embedded is not included in the calculation of micro-texture). The aggregate micro-texture statistics computed from all scans were then averaged to get the μMPD of the aggregates in the ring-shaped specimen.

Table A1 in the Appendix tabulates the micro-texture statistics for the dolomite, gravel, igneous, and limestone ring specimens on which test data were provided by TxDOT. The available data on sandstone at the time of this report were limited to only a pair of sandstone BMD and AMD ring-shaped specimens. Thus, researchers used only the test data on the dolomite, gravel,

igneous, and limestone ring specimens in evaluating the relationship between DFT friction and aggregate micro-texture.

The dependent variable in this analysis was the friction coefficient corresponding to 60 km/h (DFT_{60}), while the independent variables were the ring μMPD, aggregate type or classification, and abrasion treatment. Table 1 and Table 2 show statistical measures of central tendency and dispersion on DFT_{60} and μMPD, respectively, for the aggregate types included in this analysis.

Table 1. Central Tendency and Dispersion Statistics on DFT_{60}

Micro-Deval treatment level	Aggregate type	No. of obs.	Mean	Median	Minimum	Maximum	Std. Deviation
BMD	Dolomite	6	0.507	0.528	0.407	0.562	0.0602
	Gravel	30	0.562	0.553	0.419	0.743	0.0763
	Igneous	6	0.676	0.708	0.567	0.772	0.0842
	Limestone	34	0.534	0.541	0.352	0.682	0.0722
AMD	Dolomite	6	0.362	0.386	0.272	0.433	0.0688
	Gravel	30	0.436	0.449	0.271	0.530	0.0695
	Igneous	6	0.477	0.481	0.383	0.582	0.0682
	Limestone	34	0.333	0.337	0.151	0.501	0.0672

Table 2. Central Tendency and Dispersion Statistics on Aggregate Micro-Texture (μMPD)

Micro-Deval treatment level	Aggregate type	No. of obs.	Mean (mm)	Median (mm)	Minimum (mm)	Maximum (mm)	Std. Deviation (mm)
BMD	Dolomite	6	0.04750	0.04657	0.04230	0.05690	0.005163
	Gravel	30	0.04827	0.04792	0.04050	0.05735	0.004254
	Igneous	6	0.05463	0.05175	0.05075	0.06835	0.006831
	Limestone	34	0.05094	0.05122	0.04075	0.06200	0.005842
AMD	Dolomite	6	0.03763	0.03785	0.02780	0.04455	0.006511
	Gravel	30	0.04197	0.04215	0.03200	0.05160	0.004584
	Igneous	6	0.04258	0.04155	0.03595	0.05475	0.007078
	Limestone	34	0.03491	0.03375	0.02880	0.04415	0.004292

Table 1 and Table 2 show that DFT_{60} and μMPD diminish after the aggregates are subjected to Micro-Deval abrasion (as previously observed for μMPD in Figure 16). Researchers used the *t*-test to determine the statistical significance of the differences between the mean values of DFT60 and μMPD before and after Micro-Deval abrasion. The null (H_0) and alternate (H_a) hypotheses used for these statistical tests are, respectively:

H_0: $(\mu_{BMD})_j = (\mu_{AMD})_j$

H_a: $(\mu_{BMD})_j > (\mu_{AMD})_j$

where $(\mu_{BMD})_j$ and $(\mu_{AMD})_j$ are, respectively, the mean values of DFT_{60} (or μMPD) before and after subjecting aggregate type *j* to Micro-Deval abrasion. The results from this analysis showed that the mean BMD values of DFT_{60} and μMPD were significantly larger than the corresponding

values AMD at a significance level $\alpha = 0.05$. Table 3 summarizes the results of comparing the mean friction and texture values before and after Micro-Deval abrasion by aggregate type.

Table 3. Results from Statistical Tests of Significance between BMD and AMD Aggregate Properties.

Aggregate type	Mean DFT_{60}		*p*-value from DFT_{60} *t*-test*	Mean μMPD (mm)		*p*-value from μMPD *t*-test*
	BMD	AMD		BMD	AMD	
Dolomite	0.507	0.362	0.001541558	0.04750	0.03763	0.007803282
Gravel	0.562	0.436	5.32916E-09	0.04827	0.04197	4.19371E-07
Igneous	0.676	0.477	0.000584696	0.05463	0.04258	0.006664704
Limestone	0.534	0.333	2.39141E-18	0.05094	0.03491	5.33824E-20

** p-values indicate significantly higher mean BMD aggregate properties compared to AMD.*

Researchers used the following linear model to evaluate the relationship between DFT_{60}, aggregate micro-texture, Micro-Deval treatment, and aggregate type or classification:

$$Y_i = \beta_0 + \beta_1\,\mu MPD_i + \beta_2\,(X_{MD})_i + \beta_3\,(X_{Grav})_i + \beta_4\,(X_{LimeSt})_i + \beta_5\,(X_{Dolom})_i \qquad (1)$$

Where,

Y_i = DFT_{60} from TxDOT's test on aggregate ring *i*.

μMPD_i = aggregate ring mean profile depth (mm).

$(X_{MD})_I$ = 0 for BMD ring specimen; otherwise, 1 for AMD ring specimen.

$(X_{Grav})_i$ = 1 for gravel ring specimen; otherwise, 0.

$(X_{LimeSt})_i$ = 1 for limestone ring specimen; otherwise, 0.

$(X_{Dolom})_i$ = 1 for dolomite ring specimen; otherwise, 0.

β_0 to β_5 = model parameters determined from regression.

Note that for a granite ring specimen, $(X_{Grav})_i = (X_{LimeSt})_i = (X_{Dolom})_i = 0$. Using the Statistical Analysis System with the data given in the Appendix, researchers determined the model parameter estimates given in Table 4. The resulting relationship between friction, aggregate texture, aggregate type, and MD treatment level is given by:

$$DFT_{60} = 0.235 + 7.832\mu MPD - 0.077(X_{MD}) - 0.050(X_{Grav}) - 0.098(X_{LimeSt}) - 0.095(X_{Dolom}) \qquad (2)$$

Figure 17 compares the predicted DFT_{60} from equation (2) with the corresponding measured values. The analysis of variance statistics given in Figure 1 show that this equation is statistically significant with a coefficient of determination, R^2, of about 76 percent and a root-mean-square error (RMSE) of 0.059. Moreover, all independent variables of equation (2) are highly significant as shown in Table 4.

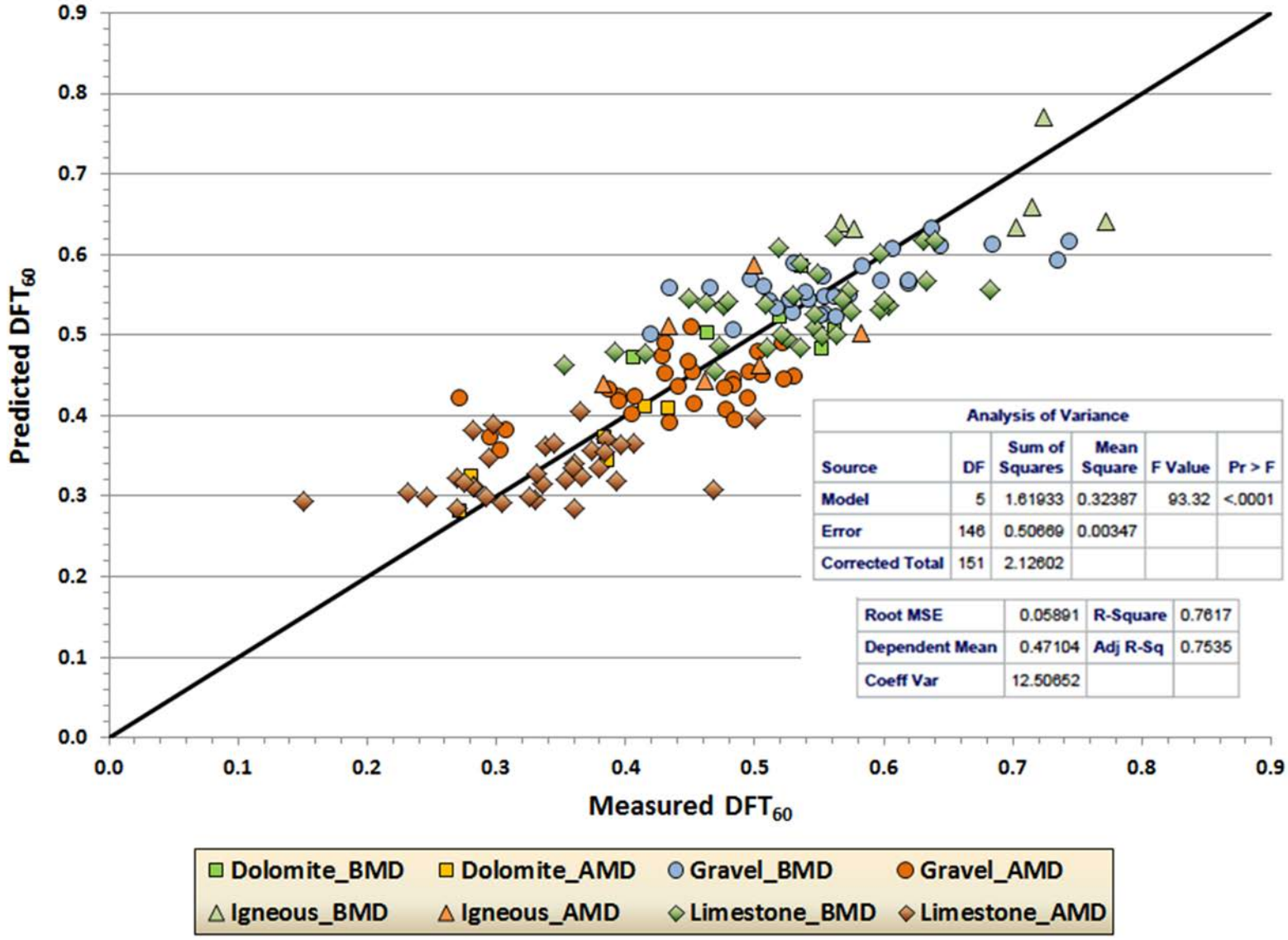

Figure 17. Comparison of Predicted vs. Measured DFT_{60}.

Table 4. Model Parameter Estimates Determined from Regression Analysis.

Predictor variable	Degrees of freedom	Parameter Estimate	Standard Error	*t* statistic	*p*-value*
Intercept	1	0.23466	0.05105	4.60	<.0001
μMPD	1	7.83185	0.88205	8.88	<.0001
X_{MD}	1	−0.07738	0.01387	−5.58	<.0001
X_{Grav}	1	−0.05011	0.01888	−2.65	0.0088
X_{LimeSt}	1	−0.09824	0.01911	−5.14	<.0001
X_{Dolom}	1	−0.09481	0.02463	−3.85	0.0002

** p-values indicate that the model parameter estimates are highly significant.*

The following effects are suggested from the given model parameter estimates:

- Aggregate micro-texture texture has a positive effect on DFT_{60} as indicated by the positive sign of the coefficient for μMPD in equation (2). A similar finding was found from an analysis of the correlation between DFT_{60} and μMPD, which yielded a positive correlation coefficient of about 0.82 between these two variables.
- Micro-Deval abrasion has a negative effect on DFT_{60} as indicated by the negative sign of the coefficient for X_{MD} in equation (2). This observation is consistent with the results of the comparisons between the mean DFT_{60} values before and after Micro-Deval abrasion. In general, lower friction coefficients were measured after the Micro-Deval.

In addition to comparing the predicted DFT_{60} with the corresponding measured values, researchers also examined the residual plots shown in Figure 18 and Figure 19 to check for outliers that could bias the parameter estimates and possibly yield to misleading results. Examination of these plots does not reveal any outliers that stand out above all others. However, since the least-squares analysis tend to pull the estimated regression response toward observations that have extreme values, outliers may not be readily detected from residual plots. To overcome this difficulty, one can evaluate the influence of an observation by omitting it in the regression analysis, and examining the change in the various estimates and statistics. This analysis can be done for each observation to assess the potential impact of each data point on the regression analysis.

To assess the influence of each observation in the data set used to determine the relationship given in equation (2), researchers used a statistic called Cook's D, which measures how much all fitted values change when a given observation is deleted from the least-squares analysis. For this analysis, a threshold of 0.5 is commonly used to identify potentially influential observations. Specifically, a Cook's D statistic greater than 0.5 identifies a data point that may be influential and worthy of further investigation.

Figure 20 plots the Cook's D statistic for each observation in the DFT-MPD data set used to determine equation (2). This figure shows that no Cook's D statistic exceeds the 0.5 threshold,

indicating no influential observations or outliers in the regression analysis based on the linear model given by equation (1).

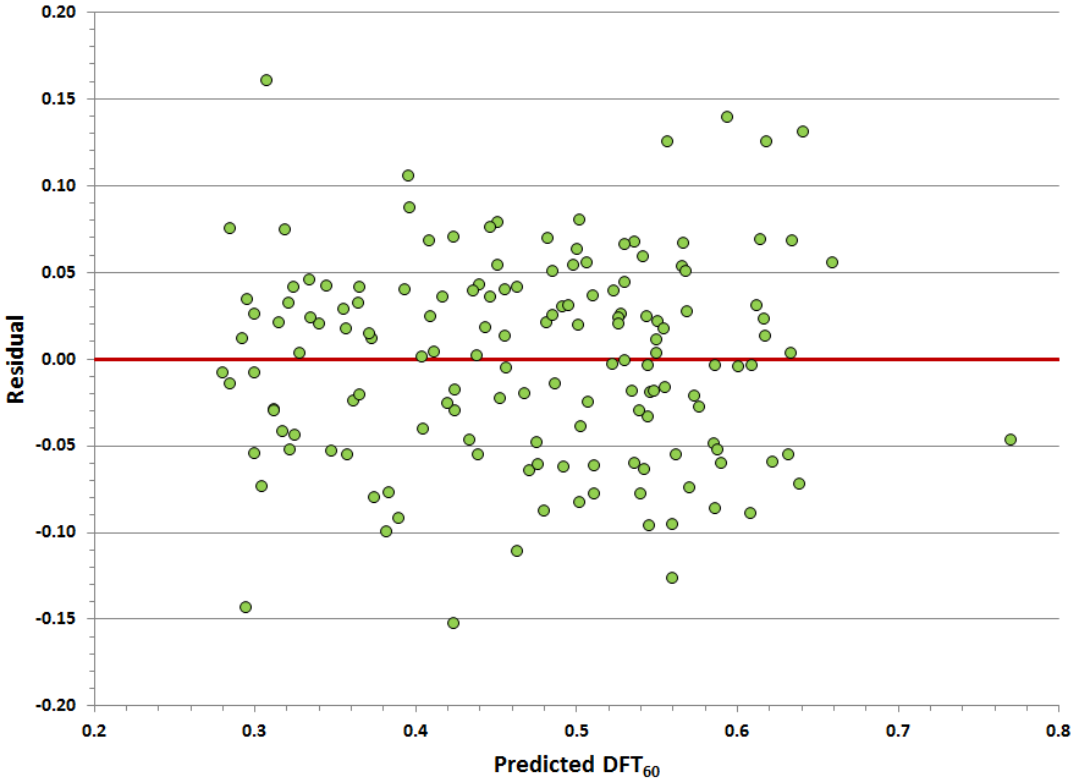

Figure 18. Plot of Residuals vs. Predicted DFT_{60}.

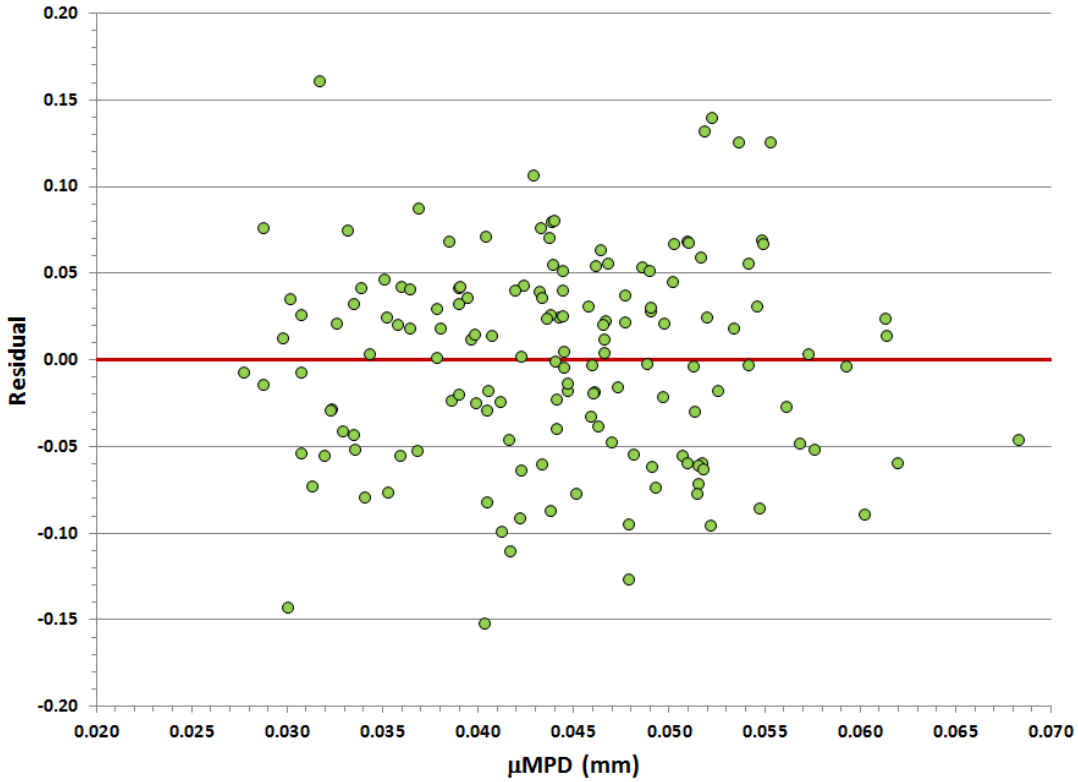

Figure 19. Plot of Residuals vs. µMPD.

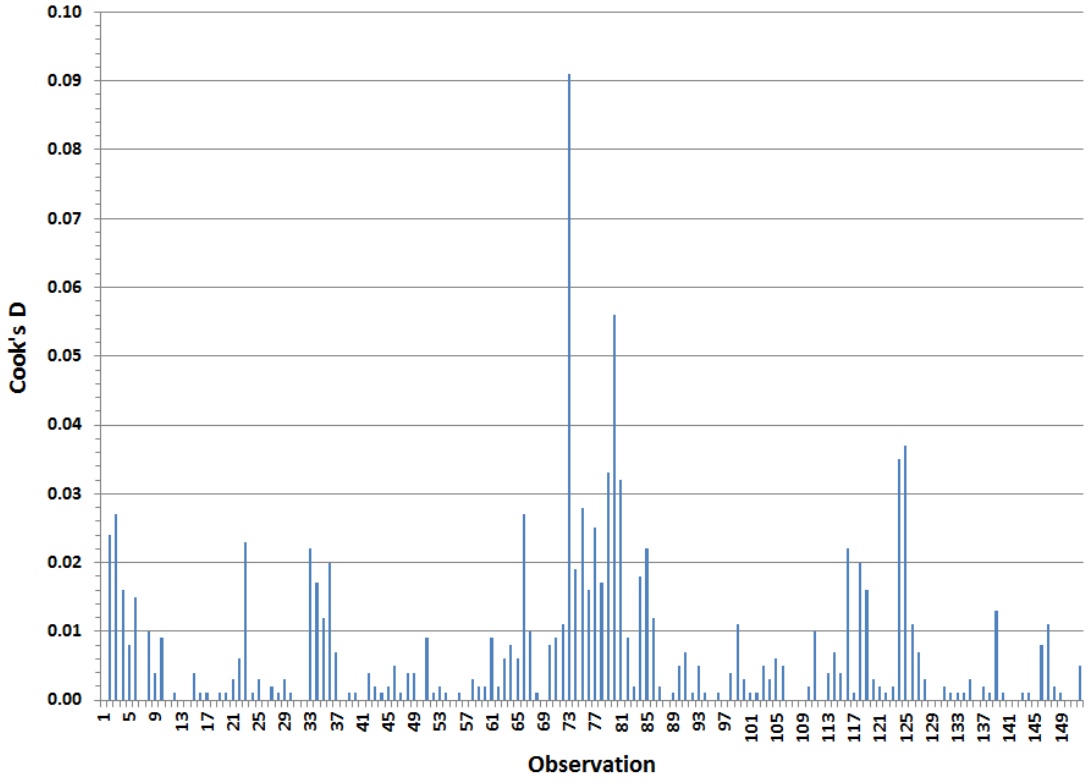

Figure 20. Plot of Cook's D Statistic for Each Observation in DFT-µMPD Data Set.

In addition to checking for outliers, researchers also checked for possible issues related to multicollinearity between the independent variables used in the regression analysis. For this purpose, researchers calculated the variance inflation factors (VIFs) associated with the independent variables. The last column of Table 5 shows the VIFs from this calculation. A VIF threshold of 10 is commonly used to flag possible issues with multicollinearity. Table 5 shows that no VIF exceeds this threshold, indicating that multicollinearity between the independent variables, all of which are also highly significant based on the *p*-values given in Table 4, is likely not of concern.

Table 5. VIFs Determined from Regression Analysis.

Predictor variable	Degrees of freedom	Parameter estimate	VIF
Intercept	1	0.23466	0.000
μMPD	1	7.83185	2.201
X_{MD}	1	−0.07738	2.105
X_{Grav}	1	−0.05011	3.730
X_{LimeSt}	1	−0.09824	3.956
X_{Dolom}	1	−0.09481	1.933

4.4. RELATIVE RANKING OF AGGREGATE TYPES

Of the aggregates tested during this implementation project, Table 3 shows that igneous aggregates have the highest mean values of DFT_{60}, both before and after Micro-Deval abrasion, followed by gravel aggregates, and then by dolomite and limestone, which appear to have comparable DFT_{60} values. To establish the significance of the differences between the friction coefficients for the aggregate types tested during this project, researchers used the *t*-test in a pairwise comparison of the mean DFT_{60} values. Table 6 summarizes the *p*-values from comparing the mean DFT_{60} for one aggregate type with that of another, both before and after Micro-Deval abrasion.

Table 6. Results from Testing Significance of Differences between Means of Measured DFT_{60} Values.

Micro-Deval Treatment Level	Aggregate Types Compared[1]	*p*-value[2]
BMD	Igneous (0.676) vs. Dolomite (0.507)	0.001538
	Igneous (0.676) vs. Gravel (0.562)	0.009485
	Igneous (0.676) vs. Limestone (0.534)	0.003680
	Gravel (0.562) vs. Dolomite (0.507)	0.041951
	Gravel (0.562) vs. Limestone (0.534)	0.071517
	Dolomite (0.507) vs. Limestone (0.534)	0.173334
AMD	Igneous (0.477) vs. Dolomite (0.362)	0.007765
	Igneous (0.477) vs. Gravel (0.436)	0.110891
	Igneous (0.477) vs. Limestone (0.333)	0.001084
	Gravel (0.436) vs. Dolomite (0.362)	0.022944
	Gravel (0.436) vs. Limestone (0.333)	5.74490E-08
	Dolomite (0.362) vs. Limestone (0.333)	0.187880

[1] *Mean DFT_{60} value given in parentheses after each aggregate type.*
[2] *p-values in red font identify cases that are significant at $\alpha = 0.05$.*

The *p*-values highlighted in red font in Table 6 identify cases where the mean values of DFT_{60} are significantly different between the given pair of aggregate types. From the results of tests done before Micro-Deval abrasion, the following observations are noted:

- The average of the measured friction coefficients for igneous aggregates is significantly higher than the corresponding averages of the measured DFT60 values for the other aggregate types.
- The mean DFT60 for gravel is significantly higher than the corresponding mean for dolomite, but is not significantly different from that of limestone.
- The mean DFT60 for dolomite is not significantly different from that of limestone.

After Micro-Deval abrasion, the results given in Table 6 suggest the following grouping of aggregate types based on the averages of the measured friction coefficients:

- Group 1: Igneous and Gravel.
- Group 2: Dolomite and Limestone.

In addition to the above analysis, researchers evaluated how the aggregate types would be ranked in terms of the predicted friction coefficients from equation (2). In this regard, Table 7 shows statistical measures of central tendency and dispersion on the predicted values of DFT_{60}. As expected from the least squares analysis to determine equation (2), the averages of the predicted DFT_{60} values are close to the corresponding averages of the measured friction coefficients given in Table 1. Figure 21 shows this expected agreement more readily. Also, the standard deviations of the predicted friction coefficients are less compared to the standard deviations of the corresponding measured values as expected from the least squares analysis.

Table 7. Central Tendency and Dispersion Statistics on Predicted Values of DFT_{60}.

Micro-Deval treatment level	Aggregate type	No. of obs.	Mean	Median	Minimum	Maximum	Std. Deviation
BMD	Dolomite	6	0.512	0.505	0.471	0.585	0.0404
	Gravel	30	0.563	0.560	0.502	0.634	0.0333
	Igneous	6	0.663	0.640	0.632	0.770	0.0535
	Limestone	34	0.535	0.538	0.456	0.622	0.0458
AMD	Dolomite	6	0.357	0.359	0.280	0.411	0.0510
	Gravel	30	0.436	0.437	0.358	0.511	0.0359
	Igneous	6	0.491	0.483	0.439	0.586	0.0554
	Limestone	34	0.332	0.323	0.285	0.405	0.0336

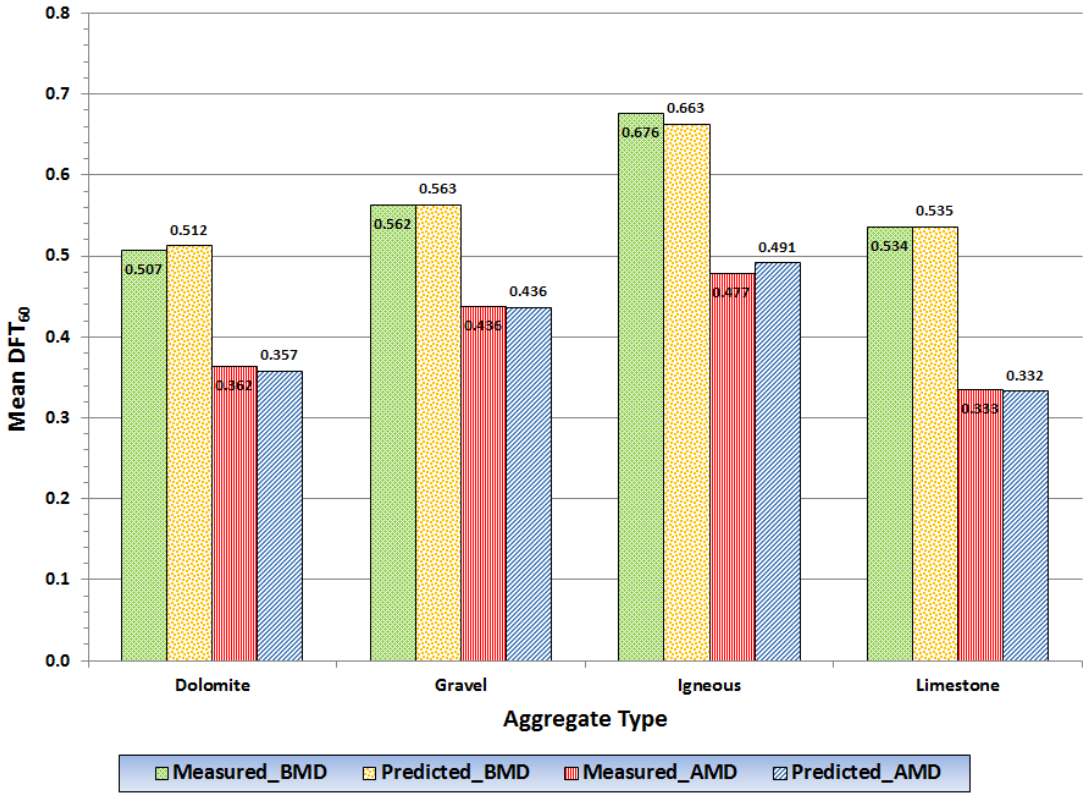

Figure 21. Comparison of Averages of Measured and Predicted Values of DFT_{60}.

A similar analysis was done to establish the statistical significance of the differences between the averages of the predicted values of DFT_{60}, and the *p*-values are summarized in Table 8. These results suggest the following grouping of aggregate types based on the averages of the predicted friction coefficients from tests done on BMD and AMD aggregates on ring-shaped specimens:

- Group 1: Igneous.
- Group 2: Gravel.
- Group 3: Dolomite and Limestone.

The above grouping may also be inferred from the coefficients of the indicator variables for aggregate type given in equation (2) and the average values of μMPDs given in Table 3. Note that for a granite ring specimen, $(X_{Grav})_i = (X_{LimeSt})_i = (X_{Dolom})_i = 0$. Thus, there is no reduction associated with aggregate type, unlike the case where the aggregate is gravel, limestone, or dolomite. Moreover, Table 3 shows that igneous aggregates have the highest mean μMPD values, both before and after Micro-Deval.

Table 8. Results from Testing Significance of Differences between Means of Predicted DFT_{60} Values.

Micro-Deval Treatment Level	Aggregate Types Compared[1]	*p*-value[2]
BMD	Igneous (0.663) vs. Dolomite (0.512)	0.000168
	Igneous (0.663) vs. Gravel (0.563)	0.002459
	Igneous (0.663) vs. Limestone (0.535)	0.000639
	Gravel (0.563) vs. Dolomite (0.512)	0.012877
	Gravel (0.563) vs. Limestone (0.535)	0.004001
	Dolomite (0.512) vs. Limestone (0.535)	0.118222
AMD	Igneous (0.491) vs. Dolomite (0.357)	0.000740
	Igneous (0.491) vs. Gravel (0.436)	0.029849
	Igneous (0.491) vs. Limestone (0.332)	0.000320
	Gravel (0.436) vs. Dolomite (0.357)	0.005592
	Gravel (0.436) vs. Limestone (0.332)	1.24002E-17
	Dolomite (0.357) vs. Limestone (0.332)	0.148544

[1] *Mean DFT_{60} value given in parentheses after each aggregate type.*
[2] *p-values in red font identify cases that are significant at $\alpha = 0.05$.*

For gravel, equation (2) shows a 0.05 reduction in the predicted friction coefficient, which is less than the reduction of 0.095 for dolomite and 0.098 for limestone. Note that the reductions for dolomite and limestone are about the same. Thus, the aggregate groups identified from the results given in Table 8 may also be partly explained from examining the aggregate type coefficients in equation (2) along with the mean μMPDs in Table 3.

While there were similarities between the rankings obtained using measured and predicted friction coefficients, there were also differences due to modeling errors, as reflected in the variability in the predictions (i.e., lack-of-fit indicated by the RMSE and R^2 values) of equation (2), as well as measurement errors.

CHAPTER 5. CONCLUSIONS AND RECOMMENDATIONS

In this implementation effort, a laser-based texture measuring system that was developed as part of TxDOT research project 0-6921 was adapted to measure micro-texture of aggregates placed on ring-shaped specimens. Samples of aggregates from five sources in their original state and subjected to Micro-Deval abrasion were set in ring-shaped molds filled with polyester. The ring-shaped specimens were tested with the adapted laser-based system—ARTS—to obtain the micro-texture characteristics followed by three repeat runs with the DFT to obtain the friction characteristics. The data processing software was also adapted to analyze the laser data and output the μMPD of the aggregates in the ring-shaped specimen configuration.

5.1. RING-SHAPED SPECIMEN PREPARATION

Researchers offer the following suggestions to be considered during the ring-shaped specimen preparation and testing:

- It is preferred that the ring being tested has a uniform distribution of aggregate particles within the ring's surface area.
- The ring should be circular in plan view (i.e., not a high degree of runout on the inner or outer diameters, and not a large error in concentricity between the inner and outer diameters).
- The mold should have uniform cross-sectional ring cavity dimensions.
- The material used to bind the aggregate particles in the ring should have a low enough uncured viscosity and high enough cured stiffness to:
  - Resist the shearing stresses associated with the DFT rubber slider.
  - Result in a relatively flat, smooth surface between the aggregate particles that is far enough below the upper surface of the particles to allow the ARTS software to pick up a reasonable portion of the rock surface above the binder. The process is somewhat similar to seal coats in which only enough binder is placed to embed the aggregate in place.
  - Epoxies and cyanoacrylates may be useful alternatives to the binders currently used.
- Preferred features of the ring mold include, but are not limited to:
  - Precision alignment system(s) that place the axis of rotation of the DFT, the ARTS hardware, and the Circular Texture Meter coincident with the axis of revolution of the ring. The more precise the alignment of these devices, the more precise the texture analysis can be relative to the true track of the DFT rubber slider.
  - A depth of the ring mold cavity that is tied to the maximum aggregate particle size being investigated. This could potentially be accomplished by using spacing rings of different thicknesses in the bottom of the ring cavity. For example, if the mold were designed for 3/8 inch (9.5 mm) nominal aggregate size, but a ¼ inch (6.35 mm) aggregate were being used, a 1/8 inch (3.18 mm) plate ring placed in the bottom of

the mold prior to specimen preparation might be an appropriate technique to improve specimen quality. The objective is to get the top surface of as many aggregate particles as possible coincident with the top surface of the mold (i.e., across the imaginary top surface of the cavity).

- A ring cavity draft angle of approximately 3° and a width at the top surface of the cavity of approximately 1.00 inch (25.4 mm).
- Since a release agent may be used in conjunction with a low friction surface such as polytetrafluoroethylene (Teflon) or ultra-high-molecular-weight polyethylene in order to facilitate removal of the sample and reuse of the mold, there may be a need to provide a mechanical enhancement to keep the bonded ring stationary (e.g., some radial serrations similar in concept to anti-vibration washers).

5.2. AGGREGATE RANKING

A relationship between friction (DFT_{60}) and micro-texture (μMPD) was developed with the results obtained in this implementation effort, which allowed predicting DFT_{60} values based on μMPD measurements, and ranking the various aggregate sources based on these characteristics. Based on both predicted and measured friction, researchers concluded:

- The mean DFT_{60} from BMD tests on igneous aggregates was significantly higher than the corresponding value for each of the other aggregate types.
- The mean DFT_{60} values from BMD and AMD tests on dolomite and limestone aggregates were not significantly different.
- The mean DFT_{60} values from AMD tests on dolomite and limestone aggregates were significantly less than the corresponding values for igneous and gravel aggregates.

Although the ranking of the aggregates based on predicted friction values obtained using the relationship between DFT_{60} and μMPD were similar to the ranking obtained with the measured DFT_{60} values, researchers recognize that more work is needed to further develop the test procedure for measuring aggregate friction, and to relate the results of laboratory tests to functional performance to establish meaningful criteria for classifying aggregates that are tied to expected skid resistance.

REFERENCES

1. Council, F., E. Zaloshnja, T. Miller, and P. Bhagwant. *Crash Cost Estimates by Maximum Police-Reported Injury Severity within Selected Crash Geometries*. Report No. FHWA-HRT-05-051, Federal Highway Administration, McLean, VA, 2005.
2. Nippo Sangyo Co., Ltd. *Dynamic Friction Tester Product Guide*, http://www.nippou.com/en/products/dft.html.

APPENDIX: DFT AND MICRO-TEXTURE DATA ON TXDOT AGGREGATE RING SPECIMENS

Table A1. Data from TxDOT Texture and Friction Tests on Aggregate Ring Specimens.

Obs. No.	Spec. ID	Aggregate Classification	MPD (mm)	X_{MD}	X_{Grav}	X_{LimeSt}	X_{Dolom}	TxDOT DFT_{60}
1	16-0784	Dolomite	0.04890	0	0	0	1	0.520
2	17-0225	Dolomite	0.04230	0	0	0	1	0.407
3	17-0269	Dolomite	0.04375	0	0	0	1	0.552
4	18-0052	Dolomite	0.04685	0	0	0	1	0.562
5	18-0102	Dolomite	0.04630	0	0	0	1	0.463
6	18-0171	Dolomite	0.05690	0	0	0	1	0.537
7	16-0784	Dolomite	0.04455	1	0	0	1	0.416
8	17-0225	Dolomite	0.03350	1	0	0	1	0.281
9	17-0269	Dolomite	0.04425	1	0	0	1	0.433
10	18-0052	Dolomite	0.03605	1	0	0	1	0.387
11	18-0102	Dolomite	0.02780	1	0	0	1	0.272
12	18-0171	Dolomite	0.03965	1	0	0	1	0.384
13	16-0855	Gravel	0.05735	0	1	0	0	0.637
14	16-0992	Gravel	0.04665	0	1	0	0	0.553
15	16-1157	Gravel	0.05175	0	1	0	0	0.530
16	17-0063	Gravel	0.04380	0	1	0	0	0.553
17	17-0068	Gravel	0.04365	0	1	0	0	0.550
18	17-0105	Gravel	0.04600	0	1	0	0	0.541
19	17-0223	Gravel	0.04670	0	1	0	0	0.572
20	17-0228	Gravel	0.04120	0	1	0	0	0.482
21	17-0243	Gravel	0.04865	0	1	0	0	0.619
22	17-0583	Gravel	0.05490	0	1	0	0	0.683
23	17-0868	Gravel	0.05230	0	1	0	0	0.733
24	17-0978	Gravel	0.04910	0	1	0	0	0.597
25	17-1243	Gravel	0.04325	0	1	0	0	0.562
26	17-1302	Gravel	0.04410	0	1	0	0	0.529
27	17-1403	Gravel	0.04595	0	1	0	0	0.511
28	17-1449	Gravel	0.04615	0	1	0	0	0.527
29	18-0003	Gravel	0.04900	0	1	0	0	0.619
30	18-0006	Gravel	0.04970	0	1	0	0	0.552
31	18-0013	Gravel	0.05420	0	1	0	0	0.606

Obs. No.	Spec. ID	Aggregate Classification	MPD (mm)	X_{MD}	X_{Grav}	X_{LimeSt}	X_{Dolom}	TxDOT DFT_{60}
32	18-0017	Gravel	0.05130	0	1	0	0	0.582
33	18-0019	Gravel	0.05535	0	1	0	0	0.743
34	18-0025	Gravel	0.04050	0	1	0	0	0.419
35	18-0040	Gravel	0.04790	0	1	0	0	0.464
36	18-0047	Gravel	0.04795	0	1	0	0	0.433
37	18-0069	Gravel	0.04930	0	1	0	0	0.497
38	18-0195	Gravel	0.04665	0	1	0	0	0.561
39	18-0201	Gravel	0.04475	0	1	0	0	0.517
40	18-0211	Gravel	0.05465	0	1	0	0	0.643
41	18-0212	Gravel	0.04735	0	1	0	0	0.539
42	18-0521	Gravel	0.04815	0	1	0	0	0.507
43	16-0855	Gravel	0.04335	1	1	0	0	0.482
44	16-0992	Gravel	0.04050	1	1	0	0	0.394
45	16-1157	Gravel	0.04905	1	1	0	0	0.521
46	17-0063	Gravel	0.03850	1	1	0	0	0.477
47	17-0068	Gravel	0.04415	1	1	0	0	0.430
48	17-0105	Gravel	0.04395	1	1	0	0	0.506
49	17-0223	Gravel	0.04705	1	1	0	0	0.428
50	17-0228	Gravel	0.04455	1	1	0	0	0.451
51	17-0243	Gravel	0.04915	1	1	0	0	0.430
52	17-0583	Gravel	0.03950	1	1	0	0	0.452
53	17-0868	Gravel	0.04245	1	1	0	0	0.482
54	17-0978	Gravel	0.04775	1	1	0	0	0.502
55	17-1243	Gravel	0.04055	1	1	0	0	0.407
56	17-1302	Gravel	0.04605	1	1	0	0	0.448
57	17-1403	Gravel	0.03785	1	1	0	0	0.404
58	17-1449	Gravel	0.04165	1	1	0	0	0.387
59	18-0003	Gravel	0.04450	1	1	0	0	0.496
60	18-0006	Gravel	0.03650	1	1	0	0	0.433
61	18-0013	Gravel	0.04390	1	1	0	0	0.530
62	18-0017	Gravel	0.04200	1	1	0	0	0.476
63	18-0019	Gravel	0.04045	1	1	0	0	0.494
64	18-0025	Gravel	0.03530	1	1	0	0	0.307
65	18-0040	Gravel	0.03200	1	1	0	0	0.302

Obs. No.	Spec. ID	Aggregate Classification	MPD (mm)	X_{MD}	X_{Grav}	X_{LimeSt}	X_{Dolom}	TxDOT DFT_{60}
66	18-0047	Gravel	0.04040	1	1	0	0	0.271
67	18-0069	Gravel	0.03410	1	1	0	0	0.294
68	18-0195	Gravel	0.03995	1	1	0	0	0.394
69	18-0201	Gravel	0.04230	1	1	0	0	0.440
70	18-0211	Gravel	0.04330	1	1	0	0	0.522
71	18-0212	Gravel	0.03690	1	1	0	0	0.483
72	18-0521	Gravel	0.05160	1	1	0	0	0.450
73	16-1211	Igneous	0.05190	0	0	0	0	0.772
74	17-0089	Igneous	0.06835	0	0	0	0	0.723
75	17-0558	Igneous	0.05160	0	0	0	0	0.567
76	17-0613	Igneous	0.05420	0	0	0	0	0.714
77	17-1226	Igneous	0.05100	0	0	0	0	0.702
78	17-1231	Igneous	0.05075	0	0	0	0	0.577
79	16-1211	Igneous	0.04405	1	0	0	0	0.582
80	17-0089	Igneous	0.05475	1	0	0	0	0.500
81	17-0558	Igneous	0.04520	1	0	0	0	0.433
82	17-0613	Igneous	0.03905	1	0	0	0	0.504
83	17-1226	Igneous	0.03650	1	0	0	0	0.461
84	17-1231	Igneous	0.03595	1	0	0	0	0.383
85	17-0041	Limestone	0.05370	0	0	1	0	0.682
86	17-0047	Limestone	0.06200	0	0	1	0	0.562
87	17-0109	Limestone	0.05025	0	0	1	0	0.574
88	17-0152	Limestone	0.04075	0	0	1	0	0.469
89	17-0180	Limestone	0.04770	0	0	1	0	0.547
90	17-0380	Limestone	0.04340	0	0	1	0	0.416
91	17-0387	Limestone	0.05495	0	0	1	0	0.633
92	17-0458	Limestone	0.06145	0	0	1	0	0.631
93	17-0472	Limestone	0.05105	0	0	1	0	0.603
94	17-0856	Limestone	0.05620	0	0	1	0	0.549
95	17-0863	Limestone	0.05340	0	0	1	0	0.572
96	17-0921	Limestone	0.05140	0	0	1	0	0.509
97	17-1000	Limestone	0.04470	0	0	1	0	0.472
98	17-1018	Limestone	0.05100	0	0	1	0	0.476
99	17-1020	Limestone	0.05220	0	0	1	0	0.449

Obs. No.	Spec. ID	Aggregate Classification	MPD (mm)	X_{MD}	X_{Grav}	X_{LimeSt}	X_{Dolom}	TxDOT DFT_{60}
100	17-1211	Limestone	0.04620	0	0	1	0	0.552
101	17-1214	Limestone	0.04580	0	0	1	0	0.526
102	17-1215	Limestone	0.04450	0	0	1	0	0.510
103	17-1237	Limestone	0.05030	0	0	1	0	0.597
104	17-1238	Limestone	0.04450	0	0	1	0	0.536
105	17-1242	Limestone	0.05765	0	0	1	0	0.536
106	17-1285	Limestone	0.05185	0	0	1	0	0.479
107	17-1287	Limestone	0.05930	0	0	1	0	0.597
108	17-1288	Limestone	0.04980	0	0	1	0	0.547
109	17-1292	Limestone	0.05260	0	0	1	0	0.530
110	17-1301	Limestone	0.06135	0	0	1	0	0.640
111	17-1316	Limestone	0.04385	0	0	1	0	0.392
112	17-1330	Limestone	0.04660	0	0	1	0	0.521
113	17-1401	Limestone	0.04645	0	0	1	0	0.563
114	17-1410	Limestone	0.05150	0	0	1	0	0.462
115	18-0022	Limestone	0.05170	0	0	1	0	0.600
116	18-0080	Limestone	0.06025	0	0	1	0	0.519
117	18-0086	Limestone	0.05200	0	0	1	0	0.568
118	18-0254	Limestone	0.04170	0	0	1	0	0.352
119	17-0041	Limestone	0.04295	1	0	1	0	0.501
120	17-0047	Limestone	0.04415	1	0	1	0	0.364
121	17-0109	Limestone	0.03910	1	0	1	0	0.407
122	17-0152	Limestone	0.03350	1	0	1	0	0.353
123	17-0180	Limestone	0.03515	1	0	1	0	0.380
124	17-0380	Limestone	0.03005	1	0	1	0	0.151
125	17-0387	Limestone	0.03175	1	0	1	0	0.468
126	17-0458	Limestone	0.04220	1	0	1	0	0.298
127	17-0472	Limestone	0.03320	1	0	1	0	0.393
128	17-0856	Limestone	0.03685	1	0	1	0	0.294
129	17-0863	Limestone	0.03585	1	0	1	0	0.360
130	17-0921	Limestone	0.03075	1	0	1	0	0.292
131	17-1000	Limestone	0.03020	1	0	1	0	0.330
132	17-1018	Limestone	0.03235	1	0	1	0	0.283
133	17-1020	Limestone	0.03865	1	0	1	0	0.338

Obs. No.	Spec. ID	Aggregate Classification	MPD (mm)	X_{MD}	X_{Grav}	X_{LimeSt}	X_{Dolom}	TxDOT DFT_{60}
134	17-1211	Limestone	0.03075	1	0	1	0	0.326
135	17-1214	Limestone	0.03360	1	0	1	0	0.270
136	17-1215	Limestone	0.02980	1	0	1	0	0.304
137	17-1237	Limestone	0.03390	1	0	1	0	0.366
138	17-1238	Limestone	0.03230	1	0	1	0	0.282
139	17-1242	Limestone	0.04125	1	0	1	0	0.282
140	17-1285	Limestone	0.03265	1	0	1	0	0.336
141	17-1287	Limestone	0.03805	1	0	1	0	0.374
142	17-1288	Limestone	0.03985	1	0	1	0	0.386
143	17-1292	Limestone	0.03900	1	0	1	0	0.397
144	17-1301	Limestone	0.03785	1	0	1	0	0.384
145	17-1316	Limestone	0.02880	1	0	1	0	0.270
146	17-1330	Limestone	0.03135	1	0	1	0	0.231
147	17-1401	Limestone	0.02880	1	0	1	0	0.360
148	17-1410	Limestone	0.03295	1	0	1	0	0.276
149	18-0022	Limestone	0.03525	1	0	1	0	0.359
150	18-0080	Limestone	0.03905	1	0	1	0	0.344
151	18-0086	Limestone	0.03435	1	0	1	0	0.331
152	18-0254	Limestone	0.03075	1	0	1	0	0.246